Global Journal of Science Frontier Research
Bio-Tech & Genetics
Volume 12 Issue 4 Version 1.0 Year 2012
Type: Double Blind Peer Reviewed International Research Journal
Publisher: Global Journals Inc. (USA)
Online ISSN: 2249-4626 & Print ISSN: 0975-5896

Crystal Structure and Kinetic Studies on Met244Ala Variant of KatG from *HALOARCULA MARISMORTUI*

By Takao SATO,Wataru Higuchi, Katsuhiko Yoshimatsu & Taketomo Fujiwara
Tokyo modify Institute of Technology, Japan

Abstract - KatG from *HALOARCULA MARISMORTUI* (*Hm*), used concomitantly with initiator (H_2O_2), exhibits high *catalase* and *peroxidase* activities with substrate (*O*DA). The distal side M244–Y218–W95 covalent adduct and M244 centered octahedral coordination complexes in the active site are essential for the *catalase* activity. Mass spectroscopic analysis of the M244A shows cleavage of the covalent adduct between Y214–W95 and M244 without its sulfer atom. Crystal structure of M244A variant in *Hm*KatG has the geometrically dimeric subunits that disrupted or not a π–interaction which is linked between heme edge (C*1C*) to the adduct end W95 (Nε*1*). The isoenzyme pattern of *peroxidase* was determined by fitting the kinetic data to non-linear (mixed) Michaelis-Menten equation and then governed by the hetero-dimeric characters. Respective *peroxidase* catalytic efficiency for two subunits was 2.5 and 4.8 -fold increased with higher binding affinity for *O*DA. It was enhanced by rotating the dihedral angle χ2 of D125.

Keywords : *Structural and Functional heterodimers/Kinetics on isoenzyme pattern of peroxidase activity / X-ray Crystallography / mass spectrometry.*

GJSFR-G Classification : *FOR Code: 060107*

Crystal Structure and Kinetic Studies on Met244Ala Variant of KatG from *HALOARCULA MARISMORTUI*

Takao SATO [α], Wataru Higuchi [σ], Katsuhiko Yoshimatsu [ρ] & Taketomo Fujiwara [ω]

Abstract - KatG from *HALOARCULA MARISMORTUI* (*Hm*), used concomitantly with initiator (H_2O_2), exhibits high *catalase* and *peroxidase* activities with substrate (*O*DA). The distal side M244–Y218–W95 covalent adduct and M244 centered octahedral coordination complexes in the active site are essential for the *catalase* activity. Mass spectroscopic analysis of the M244A shows cleavage of the covalent adduct between Y214–W95 and M244 without its sulfer atom. Crystal structure of M244A variant in *Hm*KatG has the geometrically dimeric subunits that disrupted or not a π–interaction which is linked between heme edge (C*1C*) to the adduct end W95 (Nε*1*). The isoenzyme pattern of *peroxidase* was determined by fitting the kinetic data to non-linear (mixed) Michaelis-Menten equation and then governed by the hetero-dimeric characters. Respective *peroxidase* catalytic efficiency for two subunits was 2.5 and 4.8 -fold increased with higher binding affinity for *O*DA. It was enhanced by rotating the dihedral angle χ2 of D125.

Keywords : Structural and Functional heterodimers /Kinetics on isoenzyme pattern of peroxidase activity / X-ray Crystallography / mass spectrometry.

I. Introduction

KatG is a bifurcation enzymes that catalysis *catalase* and *peroxidase*, despite differing from manmalian liver *catalase*. It, indeed, belong to a member of the class I of the plant *peroxidase* superfamily (Welinder, 1992) including the heme-containing active sites which consists of *peroxidase*-conserved amino acids at almost identical positions as in class I *peroxidase*. In *peroxidase*, compound I is reduced in two sequential one-electron transfers, usually from donor (AH) (eq. 4) and involve an intermediate called compound II (eqs. 1 and 3). Two resonance structures for compound II could coexist (eq. 2). By first one electron-transfer (ET), the donor (AH, *O*DA; *o*-dianisidine) at nitrogen atom of quinoneimine groups was excited to the *O*DA cation radical (*O*DA($^{\cdot+}$)) and then by second one ET oxidation from its intermediate can be completed to the product (A, ODA_{red}; *o*-dianisidine quinoneimine) (eq. 4).

Author α : Depertment of Life Science, Graduate school of Bioscience and Biotechnology, Tokyo Institute of Technology, 4259–B-10 Nagatsuta, Midori-ku, Yokohama, 226-8501, Japan.
E-mail : tsatoh@bio.titech.ac.jp
Author σρω: Department of Biology and Geosciences, Faculty of science, Shizuoka University, 836 Ohya, Shizuoka, 422-8529, Japan.

Compound I [Por($^{\bullet+}$)/Y218–W95($^{\bullet+}$)–Fe^{IV}=O] + AH → Compound II [Por–Fe^{IV}=O] (1)

Compound II [Por–Fe^{IV}=O] ↔ Compound II [Por–Fe^{III}–OH] (2)

Compound II [Por–Fe^{IV}=O] +AH→KatG [Por–Fe^{III}] +H_2O+A (3)

AH [*O*DA / *O*DA($^{\bullet+}$)] →A [ODA_{red}] (4)

Haloarcula *marismortui (Hm)* naturally lives in salt lake and uses sunlight as an energy source. *Hm*KatG shares 55% identity and 69% similarity in its sequence with KatG from *Mycobctrium tuberculosis* (*Mt*) as homologous protein. *Mt*KatG is interesting in its involvement of the activation of *antituberculous* pro-drug isonicotinic acid hydrazide (isoniazide, INH) (Bertrand *et al.*, 2004). INH is activated as its *peroxidase* substrate by *Mt*KatG (Zhang *et al.*, 1992; Johnsson *et al.*, 1995). Resulting radical *via* oxidation prevents growth of the pathogenic microorganism by inhibiting the synthesis of mycolic acid component of the *mycobacterial* cell wall (Heym *et al.*, 1993). Structural and functional information is available for the crystallographic, kinetics and site-directed mutagenesis studies on KatGs (Donald *et al.*, 2003; Jakopitsch *et al.,* 2004; Singh *et al.*, 2004). These structures in combination with the biochemical characterization of variants lead to identify a few of KatG-specific residues (all numbering is for *Hm*KatG), including the cross-linkage covalent adduct among W95, Y218 and M244, unique to KatGs, to coordinate G99 and Y101, D125 and E194, which is known to be mobile in KatG and which is conserved across all KatGs. It is required for [M244A] equivalent variant from *Mt*KatG to be susceptible to INH and known for *peroxidase* reaction. Hence, the M244A mutation in KatGs from *Synechococcus* PCC7942 (*Sy*) and *Bulkhorderia pseudomallei* (*Bp*) expected to be one of the commonest causes of increasing sensitivity to *O*DA and, activating significant *peroxidase* while may be remaining slightly *catalase* activities. Therefore, *Hm*KatG [M244A] variant is also expressed with an attempt at rational catalytic redesign, to elucidate *peroxidase* reaction mechanism, because this variant is expected to exhibit the equal to or higher *peroxidase* efficiency than that of Wild-type (WT) KatG. Substitution for M244A induced the significant change in the active site that

would trigger a loss of *catalase* activity and a high enhancement of *peroxidase* activity.

In this paper, *Hm*KatG [M244A] variant losts *catalase* but, indeed, reveals the higher *peroxidase* property with isoenzyme pattern that each of subunits exhibits differences between the two kinetic parameters for *O*DA (Ten-I, *et al*., 2007). This mutation also affected the structure of the access channel and therefore the enzymatic parameters for the *peroxidase* activity. The crystal structure of *Hm*KatG [M244A] variant is reported here. Remarkably, each structure of subunits was not entirely identical. Atypical correlation between the reaction rate of turnover and the substrate affinity was properly and accurately described in terms of its heterodimeric character that can performed separately from two identical subunits (designated A and B) of heterogeneous structural and functional dimer of *Hm*KatG.

II. Resource And Techniques

a) Experimental Procedures

i. *Protein Expression, Purification, Crytallization and Kinetics of the [M244A] Variant of HmKatG –*

The plasmid pHKH6 katG gene was used as the source of *catalase-peroxidase* from *Haroarcula marismortui* (ATCC43049) with a C-terminal poly-His tag. From producing the M244A substitution in KatG to yield pHKM244AH6, [M244A] variant of *Hm*KatG was prepared, purified and crystallized, as described previously (Ten-I, *et al*., 2007). Protein concentration was determined by a modified Lowry method (Dulley & Grieve, 1975) using bovine serum albumin as the standard. SDS-PAGE was carried out using the method of Schägger and von Jagow (1987). Spectroscopic measurements in the UV-visible regions were performed using a spectrophotometer model MPS2000 (Shimadzu Co., Kyoto, Japan) with a 1 cm light path cuvette. The level of heme *b* was calculated on the basis of the pyridine ferrohemochrome spectrum using a millimolar extinction coefficient of 34.4 $mM^{-1}cm^{-1}$ at 557 nm (Falk, 1964). *Catalase* activity of the purified recombinants was measured spectrophtometrically. A broad-range buffer, which was composed of 33 mM each of Na-citrate, Na-phosphate and Tris base, was used for pH adjustment of the reaction mixture at 6. The activity was determined using the reaction mixture containing 2.0 M NaCl, 10 mM H_2O_2. The reaction was started by an addition of the enzyme to the reaction mixture, decay of the absorbance at 240 nm was measured. Millimolar extinction coefficient of H_2O_2 was 0.0436 $mM^{-1}cm^{-1}$ at 240 nm (Wei *et al*., 2003). *Peroxidase* activity was measured as the reduction rate of *o*-dianisidine (*O*DA) in the presence of *tert-butyl*peroxide (*t-BuOOH*) by monitoring increase of absorbance at 460 nm. Millimolar extinction coefficient of *O*DA was 11.3 $mM^{-1}cm^{-1}$ at 460 nm (Worthington, 1988). The *peroxidase* activity was determined using the reaction mixture containing 2.0 M NaCl, 20 μM *O*DA, 100 mM *t-BuOOH* at pH8. Estimation of kinetic parameters, velocity constant (k_{cat}) and affinity constant (K_m) for *O*DA, were performed by a fit of the 22 data at each concentration to the mixed Michaelis-Menten equation (eq.5) using nonlinear regression analysis program (Sigmaplot 2000 and systat 7.0, www.systat.com, Systet Software Inc.)

$$[V]=0.5(k_{cat}^{A}\times[S]/(K_m^{A}+[S])+k_{cat}^{B}\times[S]/(K_m^{B}+[S]) \quad (5)$$

In this equation, 0.5 is coefficient constant per number heme *b* in KatG, [V] and [S] are the maximal velocity and H_2O_2 or *O*DA concentrations. The *peroxidase* isoenzyme patterns were independent of each subunit. Each of catalytic centers has significantly different kinetic parameters between subunit A (k_{cat}^{A} and K_m^{A}) and B (k_{cat}^{B} and K_m^{B}), respectively.

ii. *Digestion, Fractionation, and Sequence and Mass-Analysis of the Polypeptide –*

Endopeptidase-digestion of the two KatG recombinants was performed as follows : the purified sample (0.2 mg protein) was denatured and precipitated by treating with 5 % (w/v) trichloroacetate. The pellet that obtained centrifugatically was dissolved in 100 mM Tris-HCl buffer (pH 9.0) containing 2 M urea to become 0.2 ml in volume. Enzymatic digestion of the polypeptide was performed by treating with *lysyl-endopeptidase* (20 units, Wako Pure Chemical Industries Inc., Osaka, Japan) for 12 hr at 37 °C. Digested peptides thus obtained were fractionated by reverse-phase HPLC in 0.1% tetrafluoroacetate (TFA) with a linear gradient from 0 to 60 % (v/v) acetonitrile over 1 h at 1.0 ml/min with using cosmosil 5C18 packed column (4.6 x 250 mm, Tosoh Co.) equipped with the HPLC system (Shimadzu). N-terminal amino acid sequences of the fractionated peptides were determined by a protein sequencer model PPSQ-21A (Shimadzu). Molecular weight of the fragment was determined by ion spray ionization mass spectrometry using a single quadrupole mass spectrometer (API-150EX, Perkin-Elmer Sciex Instruments, Foster City, CA).

iii. *Structure Determination of [M244A] Variant of HmKatG –*

The crystal structure of [M244A] variant was solved by native model (PDB code 1ITK) for MOLREP (Vagin & Teplyakov, 1997). Rigid-body refinement in REFMAC5 was performed before any refinement or model building. Several rounds of positional and isotropic B-factor refinement using REFMAC5 (Vagin & Teplyakov, 1997; Murshudov *et al.,* 1997), solvent molecules were added to well defined peaks with ARP/warp (Perrakis *et al*., 1999) and manual modification were performed for the molecular model, using Xfit of XtalView (McRee, 1999). The quality of the models was analyzed using PROCHECK (Laskowski, 1993). Molecular-graphics figures were produced using PyMOL (DeLano, 2002).

iv. *Structure Based Substrate Docking and ET Pathway Analyses –*

The substrate docking and semi-empirical molecular orbital calculations were carried out with using a MOPAC2002 program (Stewart, 2002) / AM1 wavefunction (Dewar *et al.,* 1985) in BioMedCAChe ver6.1.12.34 (Fujitsu, Tokyo).

Substrate affinity was quantified by binding energy calculated from the docking study. The binding energy for a given ligand (ΔE_{ligand}) can be expressed in (eq.6) as the difference in the energy between complex and components (Fukuzawa *et al.*, 2003).

$$\Delta E_{ligand} = E_{complex} - (E_{enzyme} + E_{ligand}) \qquad (6)$$

, where are the heat of formation energy of each of three systems, i.e., E_{ligand} of H_2O_2, *O*DA (or ODA_{red}) and, E_{enzyme}, of the variant, and $E_{complex}$ of the variant complexes with H_2O_2, *O*DA (or ODA_{red}). The binding energy can be estimated to subtract the sum of heat of formation energies of each system from that of pair (of the dipartite) system, exhibiting the value of attractive interaction which is negative for MOPAC-specific calculation and can be discussed by the magnitude of its absolute value.

In addition, the ET pathway from the HOMO (the highest occupied molecular orbital; electrophilic reactivity) to the LUMO (the lowest unoccupied molecular orbital; electron affinity) were searched for the crystal structure–based analysis on the frontier electron theory (Fukui *et al.,* 1954; Fukui *et al.,* 1957) that substrate can approach to active site within 3.4Å (of van der Waals contact), when there is the energy gap within 6eV (Pearson, 1986) and the bonding orbital between HOMO of substrate with electrophilic superdelocalizability (Sr) and LOMO of reactive residue atom with nucleophilic Sr. Starting structure contained for 364 atoms of [M244A], after hydrogen addition to its crystal structure. Geometries were determined by Mechanics optimization using Augmented MM3. All the sets of molecular orbitals (HOMO to LUMO) are generated on the docking model of ligand-protein complexes which involved in the covalent adduct and heme *in vacuo*, to which ligate H_2O_2 as an initiator, *O*DA as a *peroxidatic* substrate and ODA_{red} as *peroxidase* product were bound.

v. *Fragment Analysis* -

Fragment approaches were investigated for non-covalent interactions (π-complexes) between fragment 1 (W95 or Y218-W95 adduct) and fragment 2 (heme), using the term "DFT-D3" employing BJ-damping as "DFT-D3 (BJ)" level of theory (Grimme, *et al.*, 2010; 2011). In order to estimate the hole (or electron) mobility calculation between W95 and heme, the electronic coupling term, V (eV), is defined in (eq.7) as follows:

$$V = \{J_{RP} - S_{RP} * (H_{RR} + H_{PP}) * 0.5\} / (1 - S_{RP}^2) \qquad (7)$$

, where are charge transfer intergral (hole) HOMO fragment 1-HOMO fragment 2 for J_{RP}, overlap integral (hole) HOMO fragment 1-HOMO fragment 2 for S_{RP}, site energy (hole) HOMO fragment 1 for H_{RR} and HOMO fragment 2 for H_{PP} . The term of charge transfer can be discussed by the magnitude of its square value (V^2). These calculations for charge transfer integral between WT and [M244A] were performed using the ADF2012.01 program package (Scientific Computing & Modelling)(Baerends *et al.*,2007).

III. Results

a) [M244A] variant exhibits only peroxidase activity with isoenzyme pattern–

Steady state kinetic analyses of the activities of the two recombinants were performed by using a nonlinear regression analysis. In the two subunits of WT enzyme, velocity constant (k_{cat}) of *catalase* activity revealed maximum values ($4.48 \times 10^2 \pm 54.8$ sec^{-1}; $7.75 \times 10^3 \pm 2.31 \times 10^3$ sec^{-1}) at pH 6.0. Affinity constants (K_m) for H_2O_2 were also determined as 0.130 ± 0.054 mM; 37.9±15.4mM. The *catalase* activity was completely lost by substitution of M244A; no remaining activity can be detected in this measurement system. Kinetics for *peroxidase* activity was also affected drastically by this mutation. *Peroxidase* activity of the WT enzyme showed its maximum at around pH 6.0. On the other hand, *peroxidase* activity of the [M244A] variant also revealed maximum at pH 8.0. *Peroxidase* catalytic efficiency (k_{cat}/K_m for *O*DA) for two subunits of WT enzyme was calculated as 0.650×10^6 M^{-1} s^{-1} and 0.0196×10^6 M^{-1} s^{-1}, respectively, with the coefficient of determination $R^2 = 0.999$ using 8 data points as shown in Table 1. Interestingly, in the *peroxidase* activity of [M244A] variant, relationship between the substrate concentration [S] and the rate of turnover [v] could not be interpreted by a simple Michaelis-Menten's equation. However, according to the mixed Michaelis-Menten equation (eq.5), which was derived from the model, kinetic parameters for subunit A (k_{cat}^A and K_m^A) and for subunit B (k_{cat}^B and K_m^B) were estimated by nonlinear regression analysis program. As shown in Fig. 1, the [v] is the rate of turnover and [S] are the concentration of *O*DA. [S]– [v] correlation of the *peroxidase* activity in the [M244A] variant at pH 8.0 was reproduced by using the estimated kinetic parameters for subunit A (k_{cat}^A = 1.6±0.27 sec^{-1} and K_m^A = 0.97±0.78 μM) and for center B (k_{cat}^B = 4.73±0.20 sec^{-1} and K_m^B = 50.8±7.8 μM) which is in good agreement with R^2 = 0.998. Atypical [S]–[v] curve which was explainable according to the two catalytic center model was also observed. The results indicated the enzymatic feature of the two catalytic centers in *K*atG, one (subunit A) showed low-activity and high-affinity for substrate, while the other (subunit B) is highly active but showed low-affinity.

As shown in Table 1, the substrate affinity constant of subunit B in [M244A] variant was about 7 fold higher affinity of that in the WT enzyme, whereas that of subunit A was comparable with that in the WT enzyme subunit A (k_{cat}^{A} = 0.528 sec^{-1} and K_m^{A} = 0.814 µM) and for subunit B (k_{cat}^{B} = 6.92 sec^{-1} and K_m^{B} = 352 µM). Each subunit A and B for the *peroxidase* activity is of 0.84 and 6.9-fold lower K_m value for [M244A] which is reflected in the 3.0 and 0.7-fold higher k_{cat} value as compared with those of WT. Therefore, the catalytic efficiency (k_{cat} /K_m) for *O*DA was 2.5 and 4.7-fold increase in *peroxidase* activity, respectively. It was suggested that this site mutation of [M244A] variant is fast rate of turnover for *O*DA compared with WT, by the cleavage adduct between M244-Y218-W95.

b) Identification of the Covalent-adduct and Partial Cleavage Lysyl endopeptidase-digestion and Mass-spectrometry with Reverse-phase HPLC –

To confirm with or without only a covalent link between side W95 (Cη) and Y218 (C$\varepsilon 2$) in two subunits, *Lysyl endopeptidase* digestion studies were performed for each of KatG recombinants, WT and [M244A] variant. Following proteolytic digestion, the peptide fragments were separated using reverse-phase HPLC. Fractions were collected, concentrated and submitted for Mass-spectrometry (MS) analysis. Both digests exhibit peptide elution patterns that are very similar, with notable exceptions as indicated in panel A of Fig. 2: the presence of a large peptide cluster in the retention time (r.t.) region of ~45 min in WT KatG is absent in M244A. This difference was highly suggestive of the presence of a M244–Y218–W95 covalent adduct peptide fragment in WT, predicted (from *Lysyl endopeptidase* cleavage sites) to incorporate S66–K131, A184–K235, and N 236–K249, which would be unable to form in [M224A] due to the Met→Ala mutation. Second, several additional peaks, which were not further characterized, were also observed in [M244A] but were absent in WT KatG, and may represent the above uncross-linked peptides. As the HPLC chromatograms were monitored at λ=220nm (peptide backbone), covalent adduct assignments were performed with using the characteristic spectral features and r.t. for either the M244–Y218–W95 or Y218–W95 covalent adducts. The presence of each covalent adducts were confirmed by mass spectrometry for both the M244–Y218–W95 ([S66–K131], [A184–K235], and [N236–K249]) and Y218–W95 ([S66–K131], and [A184–K235]). The M244–Y218–W95 covalent adduct that located on the distal side of the heme, is a structural characteristic common to all the KatGs. *Lyzyl endopeptidase*-digestion and fractionation by HPLC of the two recombinants, both WT KatG and [M244A] variant were performed. The polypeptide in the fraction prepared from the WT exhibited five peaks that include ions at mass/charge (m/z) for the +10 (m/z = 1474.0), +9 (1637.8), +8 (1840.1), +7 (2103.2) and +6 (2453.0) charged states by electrospray mass spectroscopic analysis (Schnölzer *et al*. 1992). Molecular weight of WT was determined as 14681.4 Da by Mass spectroscopy (MS) (upper panel B in Fig. 2). In this structure, demethylation (Cε) in the side-chain of M244 was expected; that is because the electrophilic attack of proton to the Sδ of methionine should dominate in the acidic denaturation of the enzyme by TFA. The value of mass 14681.7 Da calculated for the M244–Y218–W95 covalent adduct that combines three polypeptides ([S66–K131], [A184–K235], and [N236–K249]) is in good agreement with the experimentally determined mass of 14681.4 Da, or a mass 0.3 Da lower than the calculated value. It was indicative of the expected covalent-modification among W95, Y218, and M244 side-chains (left in panel C of Fig. 2). In case of M244A (lower panel B in Fig. 3), there are six peaks for the +10 (m/z = 1305.2), +9 (1450.0), +8 (1629.2), +7 (1863.5), +6 (2173.9) and +5 (2608.7) charged states, corresponding to that of the covalent-adduct composed of two polypeptides ([S66–K131] and [A184–K235]). We attribute this mass to a specific cleavage occurring at position M244A (i.e. loss of residues [N236-K249]) of the M244–Y218–W95 covalent adduct, whose calculated value (12958.8 Da) is also consistent with an experiment based on a mass of 12960.0 Da, or a mass 2 Da more than that calculated for the Tyr−Trp adduct. This profile indicates the presence of the Y218–W95 covalent adduct in [M244A] predicted from *endopeptidase* digest and the combination of Y218–W95 dipeptides are most likely (right in panel C of Fig. 2).

c) N-terminal sequence analysis –

The preparation for this analysis obtained from the two enzymes was shown in Fig. 3. In the sample from the WT enzyme, three amino acid residues appeared in each cycles with almost equimolar ratio, demonstrating that the sample would contain three polypeptides ([S66–K131], [A184–K235], and [N236–K249]), as predicted from *lysyl - endopeptidase* cleavage site. In case of the [M244A] variant, two residues appeared in each cycles, suggesting the presence of two polypeptides ([S66–K131] and [A184–K235]). The result also evidenced the presence of [M244–Y218–W95] covalent adduct in the WT enzyme, and the presence of [Y218–W95] adduct in the [M244A] variant.

In the M244I variant from *Mt*KatG (Ghiladi *et al*., 2005b; Ghiladi *et al*., 2005c) and *Sy*KatG (Jakopitsch *et al*., 2004), analysis of MS data has demonstrated the presence of the covalent adduct between Y218 and W95, corresponding to the result of *Hm*M244A variant. The formation of the dipeptide [Y218–W95] covalent bond has been proposed to occur upon the simultaneous on electron oxidation of both the phenol of Y218 and indole rings of W95, respectively, by KatG Compound I formation. Thus it is suggested that the

absence of a coordinate centered sulfur atom in position 244 is most likely the reason as to why the *Hm*KatG [M244A] variant did not exhibit a tripeptide [M244–Y218–W95] covalent adduct, in spite of the presence of a redox active side-chain (indole group) of N$\varepsilon 1$ atom in position 95 adjacent to heme. As only one of the INH - resistance conferring *Mt*KatG variants has been found to conclusively cause a complete lack of *catalase* activity ([R409L], Ghiladi *et al*., 2004), the result is in good agreement with study previously reported which noted any correction between drug susceptibility and the absence of the tri-peptide [M244–Y218–W95] covalent adduct.

d) Heterologously-Structured Dimer Subunits in [M244A] Variant –

The crystal structure of *Hm*KatG [M244A] variant was determined by using Molecular replacement method with WT (PDB code 1ITK) as probe molecule. Structural refinement statics are shown in Table 2. The overall structure is similar to that of the WT. The average r.m.s. deviation between each subunit are 0.67 Å for the backbone Cα atoms, respectively. For [M244A] variant, the electron density maps defined backbone and side-chain atoms of 1380 amino acid residues, two iron atoms, two heme groups and 306 water molecules in two subunits. Residues 1–29, 295–301 and 727–731 of both subunits are not included in the final model because they are invisible or suspense in the electron density map. The model has crystallographic agreement R and R_{free} factors of 28.3% and 32.5% for 71879 reflections in the resolution limit of 2.33Å. On the other hand, an asymmetric unit of [M244A] variant crystal contains two subunits A and B related by non-crystallographic two-fold symmetry. The comparison of the dimer structures in [M244A] reveals remarkable few changes, which are the relative displacement of W95, H96, D125, E194 and E222 for 1.5 Å, 0.82 Å, 0.81 Å, 0.87 Å, 0.814Å and 0.824Å significant for overall 0.49 Å r.m.s. displacement in backbone atoms.

e) Covalent-adduct, Heme Distal Side of the Active Center and Substrate Access Channel –

The electron density maps corresponding to the active centers in subunit A and B of [M244A] variant are clearly evident to be in the different state as shown in Fig. 4. In subunit A, there is no continuous electron density and a link between distal side tryptophane and tyrosine could not be found but distance between Y218 C$\varepsilon 1$ and W95 Cη is 2.42Å, suggesting the presence of covalent adduct between the Y218 and W95. By contrast, in subunit B, the distance between Y218 C$\varepsilon 1$ and W95 Cη is 1.76Å, strongly demonstrating the covalent-linkage between Y218 and W95. The lower electron density was caused by the disorder effect of mobile Y218 on the flexible LL1 loop which formed the substrate access channel into the cavity as shown in Fig.6. Such flexibility may be observed in subunit A. Moreover, A244 Cβ moves away from Y218 C$\varepsilon 2$ at 0.95Å and 0.824Å, respectively. By substitution of Met244 to Ala, the covalent adduct between M244 and Y218 was disrupted. This clearly rules out the hypothesis that M244 takes part in the integrity and/or formation of the covalent bond between Y218 and W95. Structural information obtained from X-ray crystallography on the [M244A] variants can confirm these results from MS. In this work, we have demonstrated that M244 variants affect the linkage between W95 and Y218.

f) Mobile D125

Side-chain of D125, which located at the bottom of the channel, showed remarkable structural change in the [M244A] variant. In subunit A, the side-chain D125 is hydrogen (H-) bond interaction with the backbone amino nitrogen of I217, resulted perpendicular rotation of $\chi 2$ of D125 side-chain to face the imidazole of H96 (Fig. 5). D125 in subunit B was still fixed as well as the original architecture observed in the WT enzyme by H-bonding with backone of I217 in the LL1 loop. D125 has been known to be important in the H_2O_2 oxidation to date (Jakopitsch *et al.,* 2003a; Singh *et al*., 2004). However, there is a dramatic reversal of the side chain dihedral angle $\chi 2$ of D125 without backbone distortion with respect to that of the WT structure. In subunit A, the larger dihedral angle $\chi 2$ of D125 than that in subunit B, which the side-chain of D125 is reoriented to bind *peroxidase* substrate as *O*DA or water molecule as deriving from H_2O_2, respectively. Hence, the mobile D125 residue will also be suggestive of utilizing as both initiator H_2O_2 and substrate recognition, making it effective in binding substrate, though disruption of π-complexes with heme and W95 known to act on as molecular switch from the *catalase* to the *peroxidase* (Carpena *et al*., 2005). Also the backbone amino N of I217, a proton donor, forms an H-bond to the oxygen O$\delta 1$ of the side-chain carbonyl group of D125 with displacement from at a distance of 2.69Å toward 2.80 Å, rotating by 63.8° with respect to the O$\delta 1$–Cγ–O$\delta 1$ (I217) angle. Thus it can be concluded that no H-atom is seen in the C=O$\delta 1$ group (D125). When O$\delta 2$ in the side chain of the D125 can be an ionized carboxyl group at optimum pH6 near pKa value of 4.0, it is implying that O$\delta 2$ is the –OH position and that an ionized carboxyl group of D125 cannot be proton accepter but may be a powerful proton donor for *peroxidase* substrate. Because of possible function of D125 for binding the *peroxidase* substrate, one of two catalytic centers with extremely high affinity (K_m^A = 0.974 μM) for *O*DA in M244A variant would be attributed to rotate the side-chain dihedral angle $\chi 2$ by 61.3° of the mobile D125 in the subunit A.

g) Access Channel –

While the WT exhibits *catalase* activity that can detoxify oxidative radicals, stabilizing LL1 loop by covalent adduct linkage between Y218 and M244 on

helix E, the [M244A] variant lost *catalase* activity due to the cleavage of the linkage and then the mobile upstream residues of LL1 (accompanied by the mobile D125). When the displacement of E194 and E222 was endured by the flexible response of the downstream portion of LL1 loop, it allows the mouth of the channel to open and to facilitate adequate uptake of substrate into the heme cavity. Side-chain of E194 on LL1 loop locates at the entrance of the channel and was also affected by this mutation.

h) π-complexes between W95 and Heme –

The Structural architecture of the distal residues shows significant differences between the subunit A and B. As shown in Fig.6, the distance between indole nitrogen atom of W95 (Nε*1*) and carbon atom (C*1C*) in heme pyrrole ring C is 3.87Å and 3.25Å, respectively, on the vicinity of γ- meso heme edge in subunits A and B. It is suggested that the space of heme pocket was extended in subunit A and indole ring of W95 could not form π-complexes with the porphyrin.The π interaction between the distal W95 and heme can stack and may form the ET complex, since resulting from π interaction distance that is slightly shorter 3.25Å in subunit B than the 3.3 Å distance observed in WT enzyme. According to Marcus theory, the electronic coupling term, V, depends on the distance between the electron donor (heme) and electron acceptor (W95). The electronic coupling term of WT is of high square value of 0.06836 eV^2 and 0.79315 eV^2 for subunit A and B, respectively. M244A exhibits 0.00241 eV^2 and 0.04082 eV^2 during *peroxdase cycle* , which would not almost transfer electron from Heme to W95. It is strongly sensitive to the electronic coupling term that the rate of ET in protein controls the *catalase* function.

IV. Discussion

a) Functional Prediction guided by Docking Study with H_2O_2 ,ODA (or ODA_{red}) molecule based on the structure of [M244A] –

Though K_m values (affinity) for H_2O_2 to [M244A] cannot be detected from kinetic study, the structure-based docking calculation is useful in distinguishing subunit A from B, in [M244A] variant that has binding H_2O_2 affinity. It cannot estimate only H_2O_2 affinity but can also predict the proposal space among three target residues as W95, H96 and D125. The docking energies defined as the negative value of attractive binding energy, which each subunit A and B is of (-30.3kcal/mol; -23.9kcal/mol) for W95, (-29.9 kcal/mol; -18.2 kcal/mol) for H96 and (-32.1 kcal/mol; -30.3kcal/mol) for D125 as shown in Table 3.

A calculated binding energy in the [M244A] variant (-76.5 kcal/mol for subunit A; -30.9 kcal/mol for B) also reveals to have significantly high affinity for *O*DA and a possible site has been proposed in a cavity on the distal side of the heme. Consequently, the porphyrin carbon atom (C*HB*) of δ-meso heme edge , which is in the position to make a 90-degree turn to the right from γ- meso edge of the heme plane (in Fig.6), may serve as a docking site for substrate as *O*DA or ODA_{red} (*O*DA cation radical; *O*DA ($\blacksquare^+$). However, the specific enhancements in *peroxidise* can be influenced by the *O*DA affinity difference between each subunit. The 2-fold higher energy for subunit A than that of subunit B has been predicted from docking with *peroxidise* substrate as *O*DA. The binding site of ODA_{red} had been estimated with -46.6 kcal/mol from docking calculations against D125 for subunit A but repulsion energy for subunit B in Table 3. Thus the active site of subunit A exhibits the higher affinity for the imino (>C=NH) group of ODA_{red} and deprotonate the amino (-NH_2) group of *O*DA more efficiently than that of the subunit B. The difference of catalytic efficiency in M244A here is of the 18 fold higher subunit A than that of B. Arising from the H–bonding interaction with either *O*DA or ODA_{red}, the promising *peroxidase* in [M244A] variant may result from lost *catalase* activity by a change in the localized electronic state between C*1C* and C*HB* in the heme edge.

b) Reasonableness of peroxidatic expression evaluated by [M244A] Structure- based Frontier Orbital Calculations

While the difference between WT KatG and [M244A] variant structures are very subtle changes and the structural integrity is highly maintained, the HOMO/LUMO orbital calculation appears to functioning of the enzyme. When the *O*DA binds to δ-edge of the heme estimated as of LUMO and then W95 cleavage from the γ-heme edge, KatG appears to convert from *catalase* into *peroxidase* function. As shown in Table 4, indeed, it is supported that *catalase* activity lost when ET cannot complete between C*1C* carbon Heme and Nε*1* nitrogen atom W95. Though the C*1C* carbon atoms [for subunit A of -0.96eV and B of -1.27eV] of the heme is mix of LUMO orbital with nucleophilic Sr of (0.523, 0.771) and temporary HOMO with electrophilic Sr of (0.510, 0.437), the C*1C* can either less than 3.3 Å or always link the π-π interaction to W95, if W95 Nε*1* ($\blacksquare^+$) cation radical show usually HOMO with electrophilic Sr of (0.462, 0.518) and transient LUMO orbital with nucleophilic Sr of (0.487, 0.355) on the covalent adduct of Y218–W95 [-7.57eV, respectively, and -7.62eV], since both energy gaps exceed the capacity of ET over 6 eV, having no *catalase* activity for [M244A]. Having electron-withdrawing (proton donor) group, C*HB* carbon atoms of heme are of LUMO in subunit A [-1.87eV] and B [-1.39eV] and also exhibit most active due to nucleophilic Sr of (1.113, 0.924). The most likely site of binding *peroxidase* substrate would be the C*HB* atom in the δ-meso heme edge. The *peroxidase* substrate acts as the electron donor in the *peroxidase* reaction. It is possible to recognize as the *peroxidase* substrate with the presence of the *O*DA. However, without the *O*DA in

especially subunit B of M244A, Compound I and W95 were elaborated by ET to W95 (▪$^{+}$) cation radical from Por(▪$^{+}$) via π-complex between them. When electron donation to the W95(▪$^{+}$) cation radical from(▪)C*1C* atom on Por (▪$^{+}$), compound II reverts to compound I. The working hypothesis of the present study therefore includes the assumption that expression of *catalase* function may be converted by ET pathway for *O*DA into *peroxidase* which is inherent in KatG. In subunit B, the orbital between C*1C* Heme and N*ε1* W95 become the binding orbital (in green and yellow) and promotes the bonding of π-system of between indole rings of Trp and pyrole ring of heme, which may be reclaiming compound I. In subunit A, there is no π-bonding interaction between N*ε1* W95 and C*1C* Heme. There would not be ET at all. The two electrons normally occupy in each orbital (in red and blue) are produced by the excitation of photoreaction using sunlight as energy source and therefore Heme edge become of LUMO and may have reduction of compound II when *O*DA(▪$^{+}$) radical cation bound to C*HB*.

Kinetic parameters in the *Hm*KatG [M244A] variant are determined by fitting the kinetic data to non-linear (mixed) Michaelis-Menten equation and show that isoenzyme pattern of active two catalytic center motifs typical of *peroxidases.* For crystallographic analysis of *Hm*KatG [M244A] variant indicated that KatG is a functional heterodimer in governing KatG dimeric subunits structure. Despite of missing *peroxidase* substrate, no *catalase* reactivity against the second H_2O_2 exhibits at all so that the electron cannot transfer from M244 to the covalent adducts W95 via Y218. In spite of a π-π* electron interaction of the heme with the covalent adduct W95, the ability to transfer electron between an electrophile of tyrosinate of Y218 and the nucleophile of sulfur cation was lost by the deletion mutation at the position 244. Therefore KatG is considered the *catalase* function to use a methionine nucleophile intramolecularly- and octahedrally-coordinated complex with the carbonyl O atoms of Y101 and G99. [M244A] was of not identical electron pathway in two subunits. The phenalic group of Y218 could move its side chain closer to the indole group of W95 in subunit B than that of subunit A. Subunit A disrupted a possible *π-π** interaction between W95 and heme. Including the differences in active site geometry, it would be sufficiently stronger to facilitate the oxoferryl (Fe (IV) =O) reduction in the *peroxidase* reaction. And back donation of electron from heme edge to W95 would suffice for compound I revitalization.

*O*DA binding affinity for subunit A was enhanced by χ2 of 61.3° in the carboxyl side chain of D125. On the contrary, in subunit B, the consequent ET from heme to W95 could explain the enhancement of *peroxidase* and iteratively-generated compound I intermediate. The isoenzyme pattern of *peroxidase* was discussed in terms of its hetero-dimeric character of *peroxidatic* subunit A for reduction of compound II and subunit B for reclaiming compound I. The value of catalytic efficiency (k_{cat}/K_m) for the *peroxidatic* reaction catalyzed by the *Hm*KatG [M244A] variant falls within the expected range for an efficient enzyme (Albery & Knowles, 1976).

The M244–Y218–W95 covalent adduct confirms to be essential for the *catalase* activity. It was also constructed to explore the effect of successive triple base substitutes for Met244 to Ala and to cleavage the covalent bond amongst the tri-peptide. The [M244A] variant that coupled with the structure based-evolution within laboratory time scale is not biochemically associated with INH susceptibility. *Catalase* activity of KatG prevents INH oxidation to the active form. Despite of INH resistance-conferring variants, this "unnatural" protein engineering for *Hm*KatG, can confirm the inherent *catalase* functional capability for M244 of capping the C-terminal ends of E-helix in KatG. Perhaps the most intriguing feature of the *Mt*KatG is its ability to mediate INH susceptibility. In the closing discussion, lastly the kinetic characterization of KatG enzyme in this bacterial has been detected isoenzyme pattern of *peroxidases*. For a better understanding of the complex interrelations between *catalase* and *peroxidase* and the oxidation of phenols, *peroxidases* are highly polymorphic enzymes, and the functionality of each isoenzyme depends on its (acidic) nature and its persistent growth phase of the *Mt* clinical strains. In order to facilitate the *peroxidase* activity and to understand the metabolic functions that are needed for the persistence of *Mt*, the structure based compounds can be useful in the design of HIV/anti-tuberculosis drugs that could eradicate persisters effectively.

V. Conclusion

KatG exhibits *catalase* and *peroxidase* Sulfer–centered M244 coordinated complexes with carbonyl oxygens of G99 or Y101, the covalent adduct, and π–conjugated complexes interacted with heme facilitate *catalase* reaction. It is crucial for understanding INH-sensitivity process how KatG functional groups participate in *peroxidase* catalysis.

VI. Abbreviations

INH, isoniazide, isonicotinic acid hydrazide; H_2O_2, hydrogen peroide; *t-BuOOH*, *tert*-butylperoxide; *O*DA, *o*-dianisidine, 4-(4-amino-3-methoxyphenyl)-2-methoxyaniline; *O*DA (▪$^{+}$), *O*DA cation radical; ODA_{red}, *o*-dianisidine, quinoneimine,4-(4-imino-3-methoxycyclo-hexa-2,5-dien-1-ylidene)-2 methoxycyclo- hexa-2,5-dien-1-imine; HOMO, the highest occupied molecular orbital (electrophilic reactivity); LUMO, the lowest unoccupied molecular orbital (electron affinity); Sr, superdelocaliza-bility.

VII. Data Deposition:

The atomic coordinates and structure factors have been deposited in the Protein Data Bank, www.rcsb.org (PDB ID codes 3VLM for M244A)

References Références Referencias

1. Albery, E.J., and Knowles,J.R. (1976) Evolution of enzyme function and the development of catalytic efficiency. Biochemistry 15, 5631-5640.
2. Baerends, E. J., Berger, J. A., Bérces, A., Bickelhaupt, F. M., Bo, C., de Boeij, P. L., Boerrigter, P. M., Cavallo, L., Chong, D. P., Deng, L., Dickson, R. M., Ellis, D. E., van Faassen, M., Fan, L., Fischer, T. H., Fonseca Guerra, C., van Gisbergen, S. J. A., Götz, A. W., Groeneveld, J. A., Gritsenko, O. V., Grüning, M., Harris, F. E., van den Hoek, P., Jacob, C. R., Jacobsen, H., Jensen, L., Kadantsev, E. S., van Kessel, G., Klooster, R., Kootstra, F., Krykunov, M. V., van Lenthe, E., Louwen, J. N., McCormack, D. A., Michalak, A., Neugebauer, J., Nicu, V. P., Osinga, V. P., Patchkovskii, S., Philipsen, P. H. T., Post, D., Pye, C. C., Ravenek, W., Rodriguez, J. I., Romaniello, P., Ros, P.,Schipper, P. R. T., Schreckenbach, G., Snijders, J. G., Sola`, M., Swart, M., Swerhone, D., te Velde, G., Vernooijs, P., Versluis, L., Visscher, L., Visser, O., Wang, F., Wesolowski, T. A., van Wezenbeek, E. M., Wiesenekker, G., Wolff, S. K., Woo, T. K., Yakovlev, A. L., and Ziegler, T. (2007) *ADF 2007.01, SCM*, Theoretical Chemistry, Vrije Universiteit, Amsterdam, The Netherlands
3. Bertrand, T., Eady,N.A.J., Jones,J.N., Jesmin,J.M., Nagy,J.M., Jamart-Gregoire,B., Raven,E.L., Brown,K.A. (2004) Crystal structure of *Mycobacterium tuberculosis catalase-peroxidase*. The Journal of Biological Chemistry 279, 38991-38999.
4. Carpena,X., Wiseman,B., Deermagarn,T., Singh,R., Switala,J., Ivancich,A., Fita,I., and Loewen,P.C. (2005) A molecular switch and electronic circuit modulate catalase activity in *catalase-peroxidases* EMBO Report 6, 1156-1162.
5. Dewar M.J.S., Zoebisch E.G., Healy E.F., and Stewart, J.J.P. (1985) Development and use of quantum mechanical molecular models. 76. AM1: a new general purpose quantum mechanical molecular model. Journal of the American Chemical Society 107, 3902-3909.
6. DeLano, W. L. (2002) The PyMOL Molecular Graphics System, DeLano Scientific, Palo Alto, CA.
7. Donald,L.D., Krokhin,O.V., Duckworth,H.W., Wiseman,B., Deemagarn, T., Singh,R., Switala,J., Carpena,J.X., Fita,I., Loewen,P.C. (2003)Characterization of the *Catalase-Peroxidase* KatG from *Burkholderia pseudomallei* by Mass Spectrometry. The Journal of Biological Chemistry 278, 35687-35692
8. Dulley,J.R., and Grieve,P.A. (1975) A simple technique for eliminating interference by detergents in the Lowry method of protein determination. Analytical Biochemistry 64, 136-141.
9. Falk,J.E. (1964) In: Porphyrins and Metalloproteins: Their general, physical, and coordination chemistry and laboratry methods. Biochim Biophys Acta Library Vol.2, New York, Elsevier Co, pp.181-188.
10. Fukui,K., Yonezawa,T., Nagata,C. (1954) Theory of Substitution in Conjugated Molecules. Bull.Chem.Soc.Japan, 27, 423- 427.
11. Fukui,K., Yonezawa,T., Nagata,C. (1957) MO Theoretical Approach to the Mechanism of Charge Transfer in the Process of Aromatic Substitutions. Journal of Chemical Physics., 27, 1247-1259.
12. Fukuzawa, K., Kitaura, K., Nakata, K., Kaminuma, T., and Nakano, T. (2003) Fragment molecular orbital study of the binding energy of ligands to the estrogen receptor. Pure and Applied chemistry, 75, 2405-2410.
13. Ghiladi,R.A., Cabelli,P.R., and Ortiz de Montellano,P.R. (2004) Superoxide reactivity of KatG: Insights into isoniazid resistance pathways in TB. Journal of the American Chemical Society 126, 4772-4773.
14. Ghiladi,R. A., Knudsen, G. M., Medzihradszky, K.F., and Ortiz de Montellano, P. R. (2005b) The Met-Tyr-Trp Cross-link in *Mycobacterium tuberculosis. Catalase-peroxidase* (KatG). The Journal of Biological Chemistry 280, 22651–22663.
15. Ghiladi,R. A., Medzihradszky, K. F., and Ortiz de Montellano, P. R. (2005c) Role of the Met-Tyr-Trp Cross-Link in *Mycobacterium tuberculosisCatalase-Peroxidase* (KatG) As Revealed by KatG(M255I). Biochemistry 44, 15093-15105.
16. Grimme,S.,Anthony,J.,Ehrlich,S.,and Krieg,H. (2010) A consistent and accurate *ab initio* parametrization of density functional dispersion correction (DFT-D) for the 94 elements H-Pu. *The Journal of Chemical Physics.,***132**, 154104 -154119.
17. Grimme,S.,Ehrlich,S.,and Goerigk,L. (2011) Effect of the Damping Function in Dispersion Corrected Density Function Theory.*Journal of Computational Chemistry.,***32**, 1456-1465
18. Heym,B., Zhang,Y., Poulet,S., Young,D., and Cole,S. (1993) Characterization of the KatG gene encoding *catalase-peroxidase* required for the isoniazid susceptibility of *Mycobacteriumtuberculosis.* Journal of Bacterilogy, 175, 4255-4259.
19. Jakopitsch,C.,Auer,M.,Regelsberger,G.,Jantschko, W., Furtmüller,P.G., Ruker,F., and Obinger,J.

(2003a) Distal site Aspartate is Essential in the *Catalase* Activity of *catalase-peroxidases*. Biochemistry 42, 5292-5300.

20. Jakopitsch,C.,Ivancich,A., Schmuckenschlager,A., Wanasinghe,A., Furtmüller,P.G., Ruker,F., and Obinger,C. (2004) Influence of the unusual covalent adduct on the kinetics and formation of radical intermediates in Synechocystis catalase peroxidase : A stopped-flow and EPR chracterization of the Met275, Tyr249, and Arg439 variants. Journal of Biological Chemistry 279, 46082-46095.
21. Johnsson K ,King DS, Schultz PG (1995) Studies on the mechanism of action of isoniazid and ethionamide in the chemotheraphy of tuberculosis. Journal of American Chemical Society 117 , 5009-5010.
22. Laskowski, R. A., MacArthur, M. A., Moss, D. S., and Thornton, J. M. (1993) PROCHECK: a program to check the stereochemical quality of protein structures. Journal of Applied Crystallography 26, 283-291.
23. McRee,D. (1999) XtalView/Xfit-A versatile program for manipulating atomic coordinates and electron density. Journal of Structural Biology 125, 156-165.
24. Murshudov,G.N., Vagin,A.A., and Dodson,E.J. (1997) Refinement of macromolecular structures by the maximum-likelihood method. Acta Crystallographica Section D 53, 240-255.
25. Pearson RG. (1986) Absolute electronegativity and hardness correlated with molecular orbital theory. Proceedings of the National Academy of Sciences of the United States of America. 83, 8440-8441.
26. Perrakis, A., Morris, R., and Lamzin, V. S. (1999) Automated protein model building combined with iterative structure refinement. Nature Structural Biology 6, 458-463.
27. Schnölzer, M., Jones, A., Alewood, P. F., and Kent, S.B.H. (1992) Ion-spray tandem mass spectrometry in peptide synthesis: Structural characterization of minor by-products in the synthesis of ACP(65–74) *Analytical Biochemistry* **204**, 335–343
28. Schägger,H., and von Jagow,G. (1987) Tricine-sodium dodecyl sulfate-polyacrylamide gel electrophoresis for the separation of proteins in the range from 1 to 100 kDa. Analytical Biochemistry 166, 368-379.
29. Singh,R., Wiseman,B., Deemagarn,T. Donald,L.J., Duckworth,H.W., Carpena,X., Fita,I., and Loewen,P.C. (2004) *Catalase-peroxidase* (KatG) exhibit NADH *oxidase* Activity. Journal of Biological Chemistry 279, 43098-43106
30. Stewart JJP, MOPAC 2002 release 2.1 Fujitsu Limited,Tokyo, JAPAN(2002),
31. Ten-i,T., Kumasaka,T., Higuchi,W., Tanaka,S., Yoshimatsu,K., Fujiwara,T. and Sato,T. (2007) Expression, purification, crystallization and preliminary X-ray analysis of Met244Ala variant of *catalase-peroxidase* (KatG) from the haloarchaeon *Haloarcula marismortui.* Acta Crystallographica Section F 63, 940-943.
32. Vagin,A.A., and Teplyakov,A. (1997) MOLREP: an automated program for molecular replacement. Journal of Applied Crystallography 30, 1022-1025.
33. Wei,C.J., Lei,B., Musser,J.M., and Tu,S.C. (2003) Isoniazid activation defects in recombinant *Mycobactrium tuberculosis Catalase-Peroxidase* (KatG) mutants evident in InhA inhibitor production. Antimicrobial Agents and Chemotherapy, 47, 670-675.
34. Welinder,K.G. (1992) Superfamily of plant, fungal and bacterial *peroxidases.* Current Opinion in Structural Biology 2, 388-393.
35. Worthington CC, Worthington (1988). In: EnzymeManual: Enzymes and Related Biochemicals. Freehold, New Jersey, pp.254-60.
36. Zhang,Y., Heym,B., Allen,B., Young,D., and Cole,S. (1992) The *catalase-peroxidase* gene and isoniazid resistance of *Mycobacterium tuberculosis.* Nature 358, 591-593.

Table 1 : Kinetic Constants for *peroxidase* activity associated WT *Hm*KatG and M244A variant.

All the kinetic constants was measured at Optimum pH. The averages and standard deviations were obtained from 8 individual data.

	WT		M244A	
Subunit	A	B	A	B
pH	6		8	
k_{cat} (s^{-1})	$0.528\pm5.53\times10^{-2}$	6.92±0.641	1.60±0.27	4.73±0.20
K_m(μM)	0.814±0.686	$3.52\times10^{2}\pm58.6$	0.974±0.782	50.76±7.76
k_{cat} / K_m($\times10^{6}$ M^{-1} s^{-1})	0.650	0.0196	1.645	0.092
R^2	0.999		0.998	

Table 2 : Structural refinement statistics

	M244A
Refinement	25.0-2.33
Number of reflections	71879
†Rwork(%)	28.3
‡Rfree(%)	32.5
Number of residues	1325
Number of water molecules	151
R.m.s.d.bond length (Å)	0.019
R.m.s.d.angle(°)	1.796
Average B-factor ($Å^2$)	
Protein atoms	39.79
Water molecules	32.5

‡R_{free} was calculated using a set of reflections where 10% of the total reflections had been randomly omitted the refinement and used to calculate R_{work}.

Table 3 : Binding Energies for [M244A] Variant Associated with Initiator H_2O_2 and Substrates *O*DAs.

It is suggested as binding affinity that the value of ΔE_{ligand} is negative to be predicted by docking calculation with the initiator H_2O_2 and the *Peroxidise* substrate *O*DA and ODA_{red}, according to eq.6.

M244A variant						
Subunit	A	B	A	B	A	B
	initiator		Substrate for Compound I		substrate for Compound II	
Ligand	H_2O_2		*O*DA		ODA_{red}	
Target residue						
W95 (kcal/mol)	-30.3	-23.9				
H96 (kcal/mol)	-29.9	-18.2				
D125 (kcal/mol)	-32.1	-30.3	-46. 6	repulsive	-76.5	-30.9
E194 (kcal/mol)	-22.5	-23.7	-70.0	-71.4	-67.9	-66.1
E222 (kcal/mol)	-21.2	-20.1	repulsive	-32.8	-21.2	-44.8
S305 (kcal/mol)	repulsive	-17.7	repulsive	-8.4	repulsive	-9.5
Heme (kcal/mol)	-26.6	-23.9	repulsive	repulsive	-69.3	-26.9

Table 4 : Each Subunit of MO Energy in the π-complexes with Y218-W95 covalent adduct of *Hm*KatG [M244A] Variant.

The frontier molecular orbital of (a) HOMO and (b) LUMO Energies for active site model, [M244A] variant associated with *peroxidase* reaction.

			M244A		*O*DA	*O*DA	ODA_{red}	ODA_{red}
	Subunit		A	B	A	B	A	B
reaction	*catalase*							
HOMO(cation radical) (eV)	Y218-W95 Nε1(·+)		-7.57	-7.62				
LUMO(eV)	Heme C*1C*		-0.96	-1.27				
The energy gap (eV)			6.61	6.35				
Distance (Å)			3.9	3.3				
Phase &			matching	matching				
orbital			bonding	bonding				
ET			impossible	possible				
	peroxidase							
HOMO(cation radical) (eV)					-7.522	-7.400	-7.468	
LUMO(nucleophilic) (eV)	Heme	C*HB*	-1.87	-1.39	-1.759	-1.288	-1.639	
The energy gap (eV)					5.76	6.11	5.83	
Distance (Å)					3.16	3.06	3.40	
orbital					bonding	bonding	bonding	
ET					possible	possible	possible	

Figure Legends

Figure 1 : Mixture Michaelis-Menten Plotting of *Peroxidase* activity of *Hm*katG [M244A] variant.

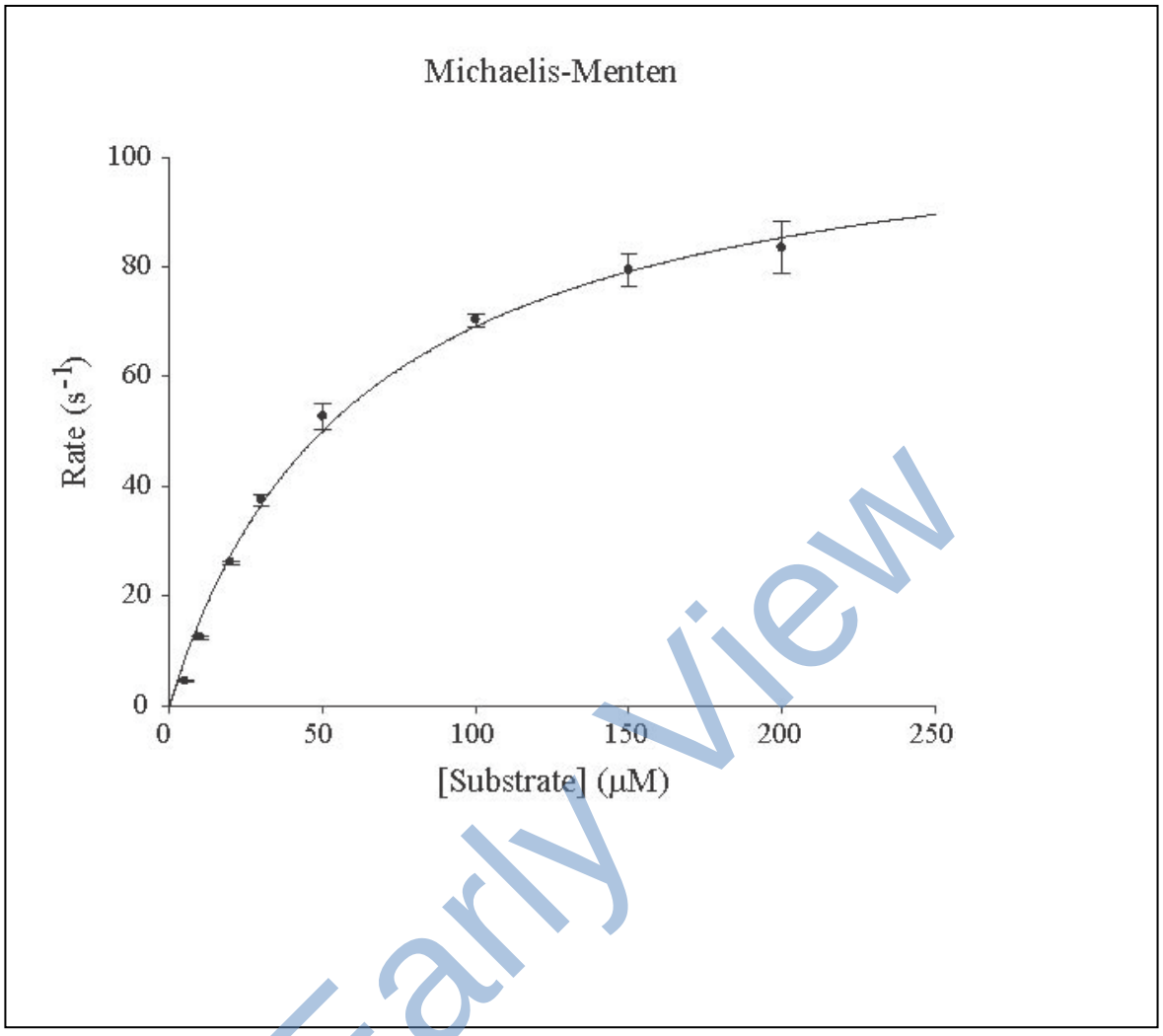

The reaction velocity [Rate, v] was plotted against the initial *O*DA concentration [Substrate, S]. Data were fitted to the Mixture Michaelis-Menten equation, yielding the kinetic parameters for the two catalytic center models (eq.5).

Figure 2 : Fractionation and Mass spectroscopic Analysis of Polypeptides Obtained by *Lysyl-endopeptidase* Digestion of WT and [M244A] variant of *Hm*KatG.

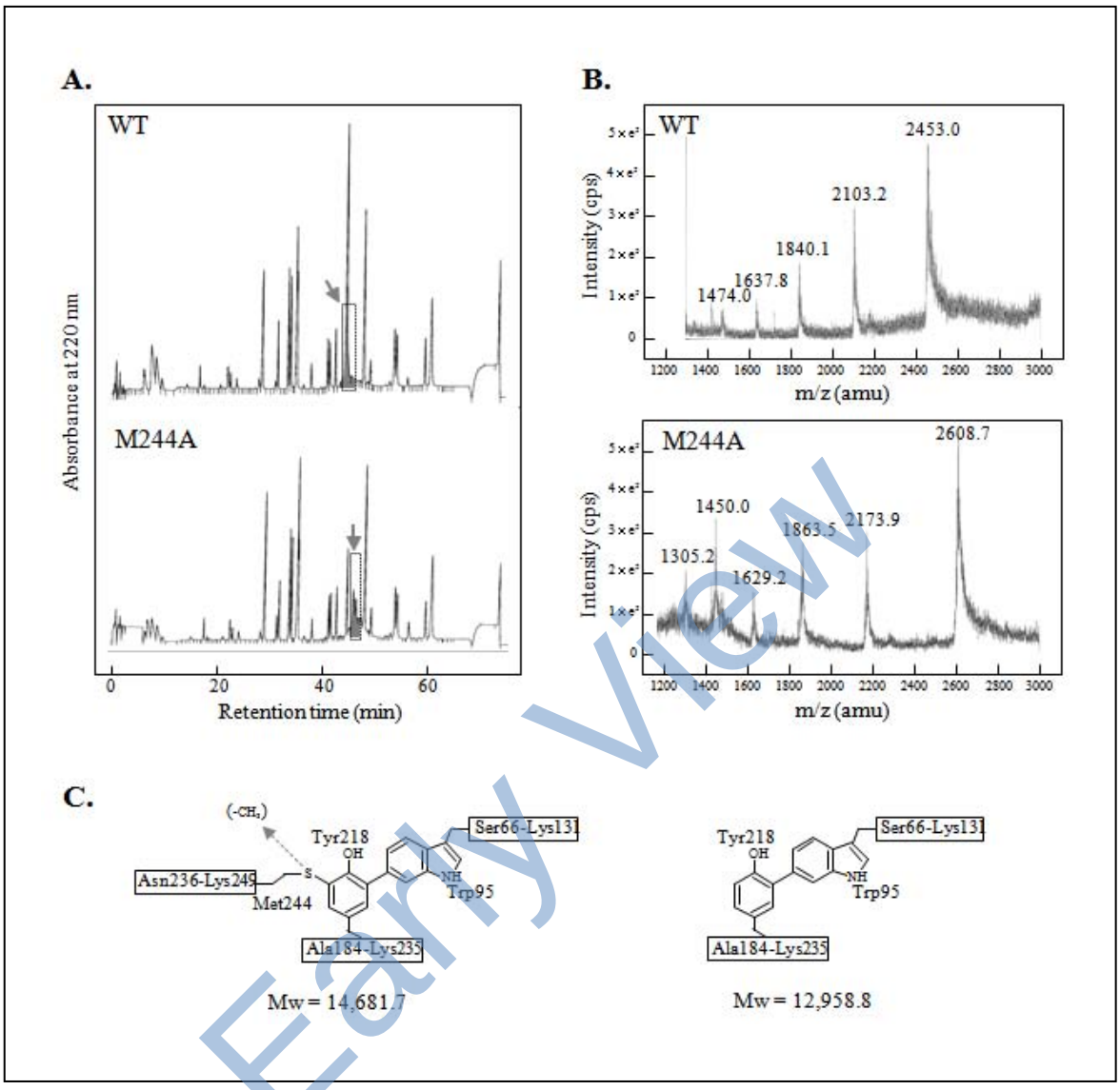

(A)HPLC chromatograms (0–75 min region) of the *lysyl-endopeptidase* digests for WT (top) and[M244A] (bottom) monitored at λ=220 nm. The region (r.t. ~45 min), corresponding to the covalent adducts, is highlighted (Fig.3, boxed area). Their fractions were corrected with the broad signals appeared at the different positions. (B) Mass spectrum (in the m/z range of 1200–3000 Da) of the covalent adducts. The polypeptide prepared for both WT (upper panel) and [M244A](lower) and was shown. (C)Fragment assignment from M244–Y218–W95 covalent adduct (left) and Y218–W95 (right).The cleavage that produced the base peak and the ion at m/z 1305.2 Da is shown in C (right).

Figure 3 : N-terminal Amino Acid Sequence of the *Endopeptidase*-digested Fragment Containing the Covalent-adduct.

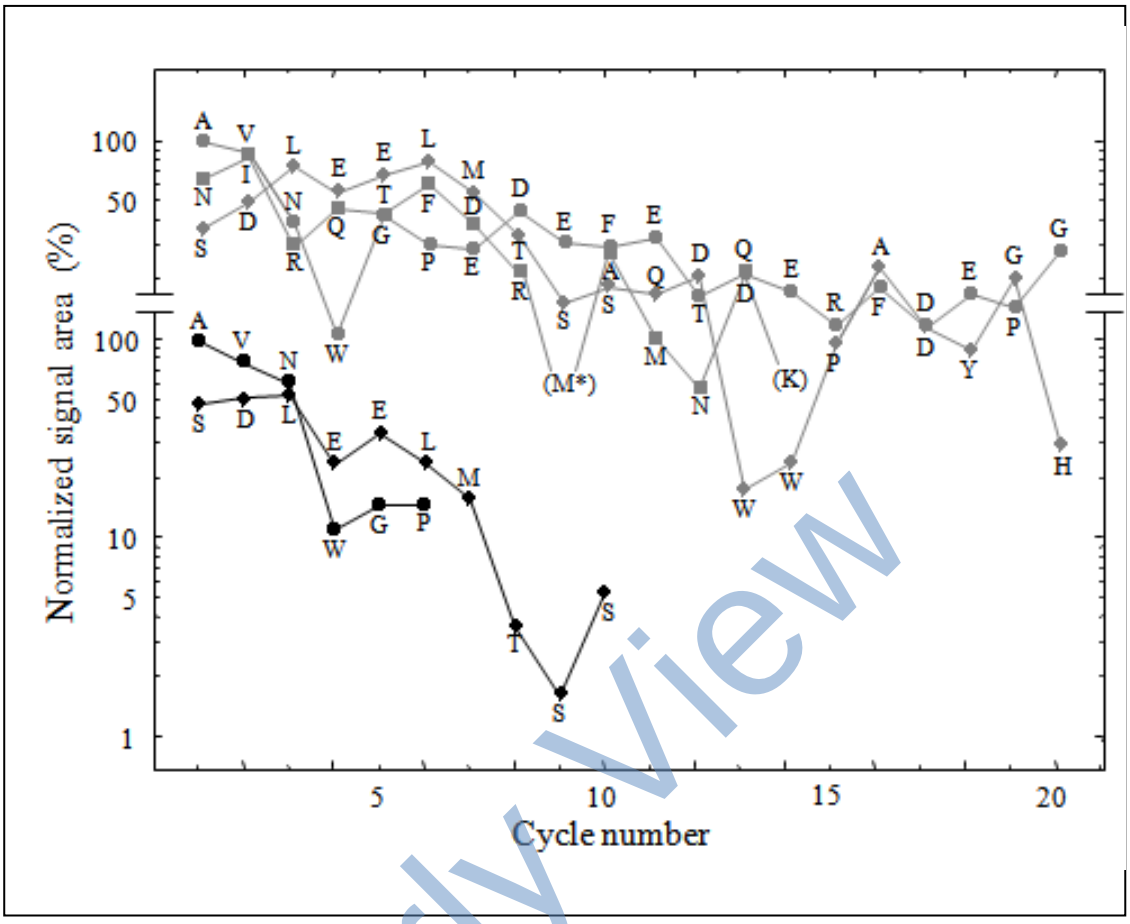

N-terminal amino acid sequence of the fragments purified from the WT (gray line) and [M244A]-variant (black line) of *Hm*KatG were analyzed. Signal areas of each residue were normalized by that of Alanine appeared at the first cycle (corresponding to A184). The signal that corresponded to M244 (M* in the figure) was not observed.

Figure 4 : The 2|Fo|-|Fc| electron density map around the covalent adduct in [M244A].

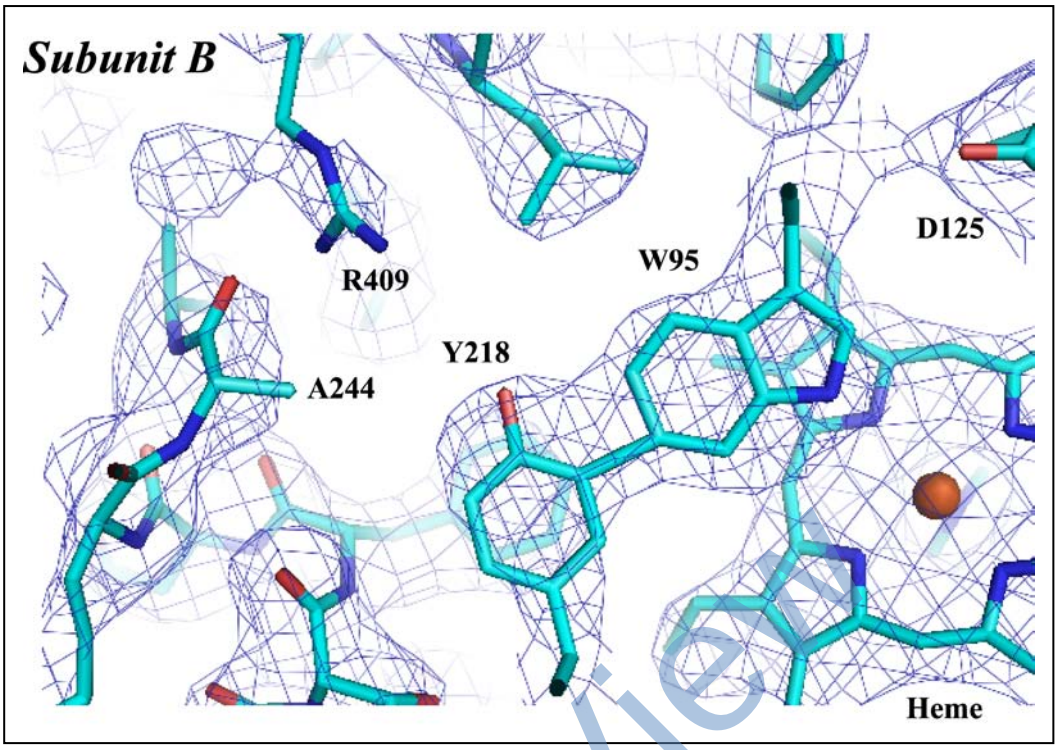

The electron density map in the vicinity of A244, Y218, W95 and heme is shown in subunit B and is contoured at 1σ (pale blue). The atom color is cyan for carbon, dark blue for nitrogen, red for oxygen and orange for heme iron. The figure was constructed using Pymol (DeLano, 2002).

Figure 5 : Mobile D125 relevant to Active Site Involving LL1 loop and Helices B, E and F in the Subunit B of [M244A] variant.

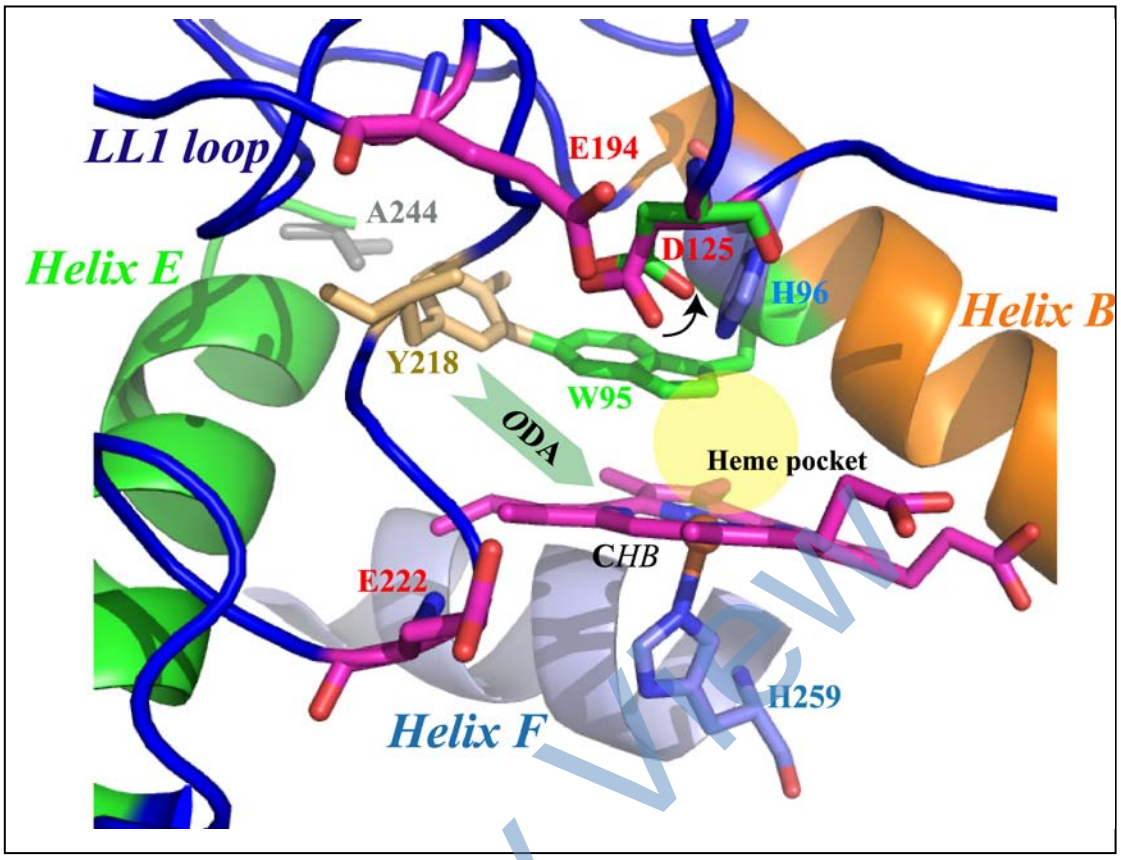

The distal H96 (on helix B; orange) and proximal H259 (on helix F; pale blue) are shown in blue. The W95 (on helix B), Y218 (on LL1 loop; cyan) and A 244 (on helix E; green) residues in green, orange, and gray. The porphyrin and its iron atom of Subunit B are represented in magenta sticks and orange sphere. The latent access channel residues of D125, E194 and E222 locate on LL1 loop, showing in red. The mobile D125 superposed that of Subunit A in WT.

Figure 6 : π-complex cleavage between W95 and Heme in subunit A of [M244A] to form *O*DA binding site.

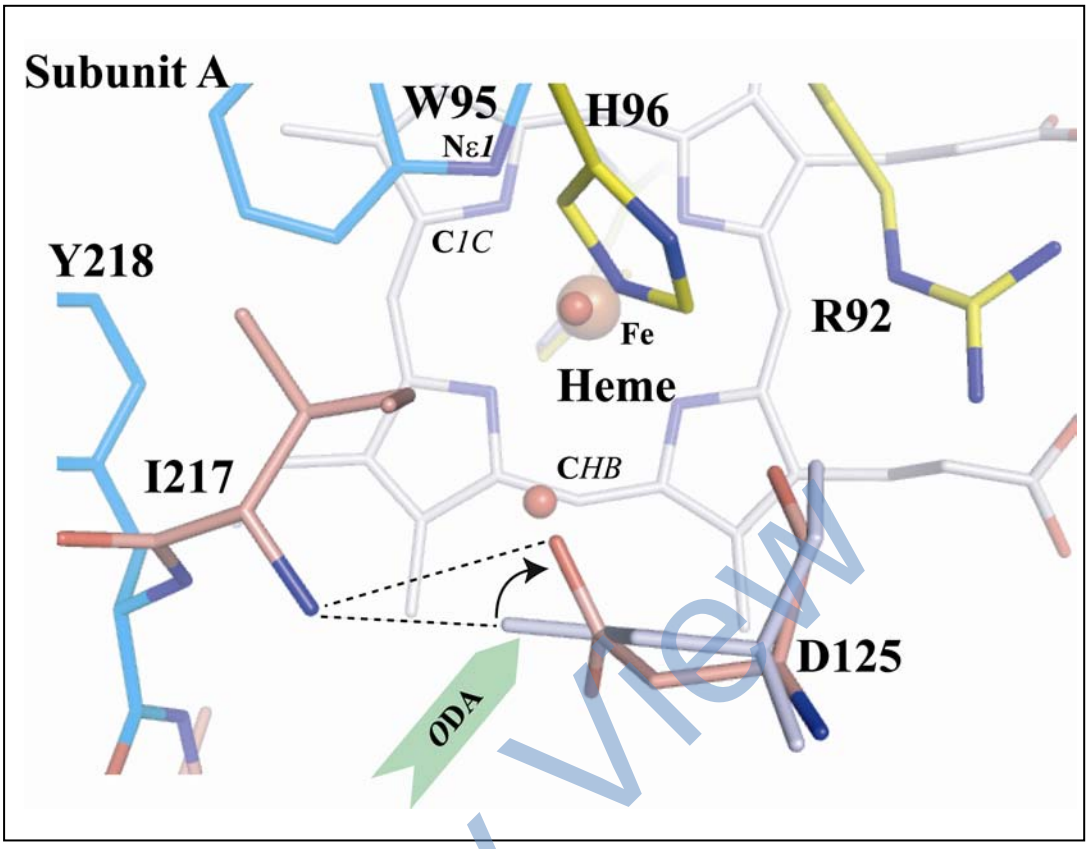

The cleavage of π-complex to W95 (N*ε1*) and γ- *meso* heme edge (C*1C*) convert from *catalase* into *peroxidase* function due to arise from the H–bonding interaction with *O*DA near the porphyrin carbon atom (C*HB*) of δ-meso heme edge, accompanied by mobility of D215. The distal R92 and H96 are presented in yellow, the Y218 and W95 covalent adduct in cyan, and D125 and I217 in pink, showing in subunit A. The nitrogen, oxygen and heme iron atoms are colored for dark blue, red, and orange. D125 in subunit B is colored blue-white and water molecule is shown as red spheres. The figure is view from the distal side of Fig 5.

Global Journals Inc. (US) Guidelines Handbook 2012

www.GlobalJournals.org